RSC Advances

ROYAL SOCIETY OF CHEMISTRY

www.rsc.org/advances

The mechanism of 2,4,6-trinitrotoluene detection with amino acid-capped quantum dots: A density functional theory study

Zhaoyang Lou,[a] Yingqi Cui,[a] Mingli Yang*[a] and Jun Chen*[b]

[a] Institute of Atomic and Molecular Physics, Key Laboratory of High Energy Density Physics and Technology of Ministry of Education, Sichuan University, Chengdu 610065, China
[b] Beijing Institute of Applied Physics and Computational Mathematics, Beijing 100081, China
*Corresponding authors. E-mail: myang@scu.edu.cn (M. Yang) and jun_chen@iapcm.ac.cn (J. Chen)

Abstract

When an amino acid-capped quantum dots solution meets 2,4,6-trinitrotoluene (TNT), it changes from colorless to red and its fluorescence is quenched. This is a recently developed technique for the detection of TNT in trace amount. However, what makes the changes in coloration and fluorescence remains controversial. Using density functional theory calculations, we studied the structures and optical properties of the products of TNT reacting with cysteine. Two compounds, namely Meisenheimer complex and TNT anion, which are respectively from an addition reaction and an acid-base reaction, were characterized, but neither of them can be used solely to interpret the experiments. Our calculations proposed the possibility of their coexistence in the solution from their similar thermodynamic stability, their predicted absorption and vibrational spectra. The superposition of their calculated optical absorption spectra produces band distributions similar to the experiments. Moreover, the measured Raman spectra that had ever been used to characterize the formation of Meisenheimer complex can not exclude the formation of TNT anion whose characteristic vibrations are buried by those of the former. Our calculations also revealed that in the Meisenheimer complex the electron delocalization in the phenyl ring of TNT is blocked by the attached cysteine, while in the TNT anion the removal of hydrogen atom enhances the electron delocalization and leads to a redshift of its first excitation in comparison with that of the Meisenheimer complex. Therefore, the key in the TNT detection is to control the QD size so as to adjust their emission at the wavelength around the absorption bands of either Meisenheimer complex or TNT anion that are formed with TNT and amino acid.

1 INTRODUCTION

2,4,6-trinitrotoluene (TNT) is an important energetic material widely used in industrial, agricultural and military affairs. It has definitely affected our life from social and personal security to environmental ecology.[1-3] Its residues have been detected in soil, groundwater, even in various food chains, threatening the human health because of their high toxicity and denaturation to our bodies.[4-6] A simple, sensitive, and cheap detection to TNT is therefore desired.

Up to now, the TNT detection is mainly on the basis of fluorescence,[7-21] Raman scattering[22-29] and electrochemical[30-36] techniques among which the fluorescent detection technique has attracted considerable attentions recently owning to its strongpoint of high signal output, sensitivity and simplicity.[37-40] The rationale of fluorescent detection is that the fluorescence of reagents changes, shifts or quenches when they meet TNT. TNT is electron-deficient due to the presence of three nitro groups and tends to interact with the electron-rich materials such as some amino acids through a charge-transfer interaction or reaction.[41] Many experimental works have reported the formation of such charge-transfer complexes that are responsible for the fluorescent shift or quenching.[11, 15, 42-44] However, what the formed complexes are remains controversial. For example，Dasary et al.[26] reported a highly selective and ultra-sensitive, cysteine (Cys) modified gold nanoparticle base label-free surface enhanced Raman spectroscopy (SERS) probe for TNT detection at a 2 pico molar level in aqueous solution. The TNT solution varied in coloration from colorless to red when Cys was added. The authors believed the formation of Meisenheimer[7, 41, 45-47] complex through a covalent addition of nucleophiles to a ring carbon atom of electron-deficient aromatic substrates. The Meisenheimer complex has optical absorptions at about 520 nm and 630 nm, appearing red in solution. However, the absorption at 630 nm has not been observed by other authors for similar systems. Tu et al.[15] prepared Mn^{2+}-doped ZnS nanocrystals with a cysteamine-capping layer and used them for the fluorescence detection of ultratrace TNT by quenching their strong orange Mn^{2+} photoluminescence. Two absorptions at 465 nm and 515 nm were observed when cysteamine was added into TNT solution, and the solution becomes red. The formation of TNT anions through an acid-base reaction was proposed. The overlap of

the absorption band of the TNT anions with the emission of Mn-doped ZnS QDs leads to the fluorescence quenching of the nano solution systems. Zou et al.[42, 43] synthesized Cys modified Mn^{2+}-doped ZnS and Co^{2+}-doped quantum dots to image ultratrace TNT in water, and observed absorptions at 465 nm and 512 nm after adding TNT into the prepared QD solution. Interestingly the authors proposed the formation of Meisenheimer complexes that quench the fluorescence emitted by the Mn^{2+}- or Co^{2+}-doped ZnS QDs.

It has no doubt that a complex is formed when TNT meets Cys. The complex may absorb the QDs' fluorescent emission and/or leads to the variation in coloration. However, there are two explanations to the mystery complex, Meisenheimer complex through a covalent bonding between the electron-deficient TNT[11, 48-50] and the electron-rich Cys or TNT anion through an acid-base reaction between the acidic Cys and the basic TNT.[15, 43, 51] Stimulated by the experimental works, we studied the interaction of molecular TNT with Cys, and the structure and optical absorption of the TNT-Cys complex by means of density functional theory (DFT) calculations, aiming to make an interpretation to the experimental observations including the color change and the fluorescence quenching of TNT-Cys-QD solutions. The understanding to the TNT detection rationale is certainly important to the development of its detection techniques and to the preparations of new semi-conducting QDs with proper fluorescence emissions.

2 Computational method

All computations were carried out with Gaussian09[52] package. First, four functionals, PBE0,[53] M06-2X,[54] B3LYP,[55-57] and ωB97xd[58] and the 6-311++G(d,p) basis set were used to optimize the TNT structure and compute its excitation energy in acetonitrile. Cooper et al.[59] measured the absorption of TNT in acetonitrile and found a strong absorption peaking at 230 nm and a small absorption band over 300 nm. Our calculated results are presented in Fig. 1. Both M06-2X and ωB97xd reproduce the peak at 230 nm, while PBE0 and B3LYP underestimate the excitation energy. However, ωB97xd also predicts a strong absorption at 159 nm, which was not observed in the experiments. Therefore, M06-2X produces better results than the other three functionals and was selected in the subsequent calculations. Next, starting from the optimized TNT and Cys structures, several TNT-Cys complexes including the

Meisenheimer complex were designed and optimized at the M06-2X/6-311++G(d,p) level. Frequency calculations at the same level were conducted for the lowest-energy structure to ensure that they are true minima on the potential energy surfaces. Finally, time-dependent DFT (TDDFT) calculations were performed to simulate the optical absorption of the Meisenheimer complex and the TNT anion and compare them with the experiments available. The linear response polarizable continuum model[60, 61] (LR-PCM) was used to mimic the solvent effect in all the calculations. The solvents were defined as the same with experiments.

3 Results and discussion

3.1 Structures of TNT-Cys complexes

Two of the designed TNT-Cys structures, the Meisenheimer complex and dehydrated TNT (**S1** and **S2** hereafter), were found much more stable than the others. These two structures, **S1** and **S2**, which are also the complexes previously suggested by experimentalists,[15, 26, 47, 49, 62] are formed through the reactions depicted in Scheme 1. Path I is an addition reaction in which the amine-N of Cys attacks the C1 in TNT and leads to **S1**. Reaction II is an acid-base reaction in which one of the methyl-H atoms is taken by the nucleophilic amine-N, and these two parts form **S2** via two hydrogen bonds.

The optimized structures of **S1** and **S2** are shown in Fig. 2, while the other less stable isomers are presented in the Electronic Supplementary Information (ESI). Table 1 lists the selected bondlengths and bondangles of **S1** and **S2** obtained with M06-2X/6-311++G(d,p), as well as those of TNT and Cys for comparison. A covalent bond about 1.56 Å in length and 0.69 in bond order was predicted between Cys-N and TNT-C1, indicating it a typical C–N single bond. Accordingly, the conjugated phenyl ring is partially deconstructed. C1–C2, C1–C6, and C1–C7 elongate remarkably, while the other C–C bonds vary about ±0.02 Å. Comparing with the TNT structure, C1 changes from sp^2 to sp^3 hybridization. The conjugation path is thus blocked at C1. The bondlengths and bondangles near to C1 are subjected to greater distortion than the others, as reflected by the geometrical parameters in Table 1. In addition, the amine-H is about 1.95 Å from one of the nitro-O, which is a typical HB.

In **S2** the removal of one proton from the methyl leads to a considerable change to the

conjugated phenyl ring. First, the methyl-C changes from sp^3 to sp^2 hybridization, shortening C1–C7 from a single bond to a double bond. C7 retains in the phenyl plane. Accordingly, the aromatic phenyl ring changes into a quinoid structure with alternatively short and long C–C bonds. C2–C3 and C5–C6 are apparently shorter than C1–C2, C1–C6, C3–C4 and C4–C5.

Table 2 lists the computed energy and Gibbs free energy changes (ΔE and ΔG) of Reactions I and II. The predicted ΔE values are rather small (less than 3.4 kcal/mol in absolute value at the M06-2X level and 5.2 kcal/mol at the PBE0 level) for both reactions. The opposite signs of ΔE for Reaction I, negative (-3.3 kcal/mol) by M06-2X and positive (4.1 kcal/mol) by PBE0, are a reflection of their small magnitudes around zero. Both reactions have positively small ΔG, indicating that extra energy is required for their proceeding. Such small amount of energy can be served either by heating or illumination in experiments. The formation of both **S1** and **S2** is therefore feasible under ambient conditions although they are thermodynamically less stable than the reactants. On the other hand, **S1** and **S2** have similar ΔE and ΔG values (the differences are only 5.5 kcal/mol for ΔE and 1.9 kcal/mol for ΔG), implying that they have similar thermodynamic stability. It is then possible that both **S1** and **S2** coexist in the system.

3.2 Optical absorption

Either **S1** or **S2** had been considered as the key compound responsible for the fluorescence quenching of semiconducting QDs and the color change of TNT-amino-QD solution.[15, 26, 49, 51] Starting from the optimized **S1** and **S2** structures, we computed their optical absorption spectra with TDDFT calculations at the M06-2X/6-311++G(d,p) level. Table 3 presents the first and second excitations and their oscillating strengths of **S1** and **S2**.

First, both TNT and Cys have their absorption in the ultraviolet region, 310 nm for TNT and 203 nm for Cys, with no effect on the color of solutions. One more possibility was considered here. TNT and Cys may form a complex via hydrogen bonds (**S3** in Fig. 2). As shown in Fig. S3 in the ESI, two HBs are formed between TNT and Cys with ΔG(298 K) = 3.5 kcal/mol. Its predicted first excitation is at 311 nm in water. Therefore, the assembly of TNT with Cys via HBs should not be responsible for the observed fluorescence quenching or color change in the visible region either.

The computed first peak of **S1** is at 451 nm, lying in the visible region. The second peak is at 340 nm, lying in the ultraviolet region. For **S2**, its first two peaks are at 508 nm and 408 nm. Neither **S1** nor **S2** has the absorption band distribution matching the observed spectra in experiments. In Zou's[50] measurement two new bands, the strong one at 465 nm and the weak one at 516 nm, were observed when TNT was added into a Cys-modified ZnS QDs aqueous solution. Similar spectra were also obtained by Tu et al.[15] It is interesting to note that although the computed absorption spectra of either **S1** or **S2** do not comply with the measurements, they possess most of the measured bands when they come together. As our calculations on the thermodynamic properties of **S1** and **S2** suggest the possibility of their coexistence in the solution, it is interesting to see the combination of their absorption spectra. Fig. 3 displays the optical absorption spectra of **S1**, **S2** and their combination at a 1:1 ratio. The superposition of the spectra of **S1** and **S2** comes to a curve, which is very close to the observed one[15, 50, 51, 63] in band locations and shapes. The two bands at 447 nm and 506 nm are in accordance with the observed ones[15,50] at about 465 nm and 515 nm.

Both TNT and Cys-capped QD solutions are colorless since they do not have absorption in the visible region. However, **S1** and **S2** are formed when these two solutions meet together. **S1**, the Meisenheimer complex, is responsible for the absorption around 460 nm, while **S2** for the absorption around 520 nm. This is why the mixture becomes red. The absorption and emission of Cys-capped QDs vary with the QD size, the capping ligand and the dielectric constant of solvent. The QDs in the measurements are about 3–50 nm in diameter, with emission at 400–600 nm.[15, 17, 42, 50, 51, 62] It is obvious that the size of QDs can be controlled to have emissions near to the absorption bands of **S1** and **S2**. This is why the fluorescence of Cys-capped QDs is quenched in TNT solution. Our calculations revealed that the key in the TNT detection is to control the QD size so as to adjust their emission at the wavelength around the absorption bands of the complexes formed with TNT and amino acid.

In addition, we computed the optical absorption of TNT anion (**S4** in Fig. 2) in the absence of the protonated Cys. Its first two peaks are at 523 and 404 nm respectively, which are very close to those of **S2**, indicating that the electron excitations in **S2** are mainly contributed by the TNT anion moiety and the hydrogen bonding that binds TNT anion and protonated Cys together has rather limited effect on the absorption spectra.

The absorption band shifts of **S1** and **S2** can be interpreted from their electronic structures. Our calculations revealed that the first excitations of both **S1** and **S2** correspond to the transitions from their highest occupied molecular orbitals (HOMO) to their lowest unoccupied molecular orbitals (LUMO). The HOMO-LUMO gaps are 5.04 eV for **S1** and 4.62 eV for **S2**, complying with the first peak locations in their absorption spectra. Fig. 4 compares the HOMO and LUMO contours of TNT, **S1** and **S2**. Both the HOMO and LUMO of TNT are mainly contributed by the conjugated phenyl ring, while the bonded nitro and methyl groups are also partially involved in the transition. The reaction with Cys, either Path I or Path II, destabilizes the TNT structure and shifts its electronic excitation to the long-wavelength direction. In **S1**, the conjugation in the phenyl ring was partially broken by the Cys addition. Its HOMO and LUMO are localized in the conjugated moiety. In **S2**, the proton removal changes the phenyl from an aromatic structure to a quinoid structure in which the conjugation path remains. Its HOMO covers all the atoms in the quinoid structure and its LUMO is also contributed from part of the atoms in the quinoid structure. The HOMO-to-LUMO transition in **S2** is therefore energetically more favorable than that in **S1**. This is why **S2** has its first absorption at a longer wavelength than **S1** does. It is also revealed from Fig. 4 that the Cys part itself is not involved in the electronic excitations, but it affects the excitation by changing the electronic structure of the TNT part.

3.3 Raman spectra

As IR and Raman spectra had ever been used to characterize the existence of either Meisenheimer complex or TNT anion in a TNT-amino-QD solution,[26, 43, 51, 63] we computed the vibrational spectra with IR and Raman intensities of **S1** and **S2** at the M06-2X/6-311++G(d,p) level and compare them with the measurements. Fig. 5 shows the computed vibrational spectra of TNT, Cys, **S1** and **S2**. Most of the bands of **S1** and **S2** can be characterized by comparing with the TNT and Cys spectra. Affected by Cys, almost all the bands of TNT shift toward the low wavenumber direction. For example, the strongest band that is associated with NO_2 symmetric stretching vibration is at 1480 cm^{-1} in TNT, but shifts to 1314 cm^{-1} in **S1** and 1300 cm^{-1} in **S2**. In addition, some bands have their relative intensity and relative wave number changed significantly. Again, we take the NO_2 symmetric stretching vibration as an

example, which is a single band at 1300 cm^{-1} in **S2**, but split into two bands at 1460 and 1480 cm^{-1} in TNT, and the separation between the two bands widens to 72 cm^{-1} in **S1**.

Even though significant variations in the spectra among TNT, **S1** and **S2** were noted, most of the bands of TNT can be traced in the **S1** and **S2** spectra. In addition to the characteristic peaks of nitro groups, the aromatic C=C stretching (at about 1700 cm^{-1}), the C_6H_2–NO_2 stretching (979 cm^{-1} in TNT, 989 cm^{-1} in **S1** and 992 cm^{-1} in **S2**) and the C_6H_2–C stretching (1257 cm^{-1} in TNT and 1080 cm^{-1} in **S1**) can be clearly identified in the spectra. The strong bands in Cys are associated with C–H, N–H and S–H stretching, respectively. These bands become much weak in **S1** and **S2** in comparison with the strong bands of TNT part.

The formation of **S1** is featured by the C1–N bond, which is at 857 cm^{-1} in Fig. 5c. Upon its formation the C1–CH_3 bond is weaken from 1257 cm^{-1} to 1080 cm^{-1}, and the N–H stretching in Cys shifts from 3542 cm^{-1} to 3354 cm^{-1}. The formation of **S2** is featured by the newly formed C1=CH_2 bond, which peaks at 1714 cm^{-1} and has similar vibrational frequency with the other C=C stretching vibrations in the aromatic ring. The N–H stretching vibration in the newly formed NH_3^+ group is at 3269 cm^{-1}.

In the Raman spectra measured by Dasary et al.[26] a strong broadband was observed at 2900 cm^{-1}, which was assigned to the NH_2 symmetric stretching, C–H stretching and CH_2 asymmetric stretching in the Meisenheimer complex. The TNT peaks are at 1615 cm^{-1} for the C=C aromatic stretching vibration, at 1360 cm^{-1} for the NO_2 symmetric stretching vibration, 1210 cm^{-1} for the C1–CH_3 vibration, etc. Because the measurement was conducted in the presence of gold nanoparticles, the observed bands should be to somewhat different from our calculations. The shifts are about 50–110 cm^{-1}. However, one can still note that all the new vibrational bands featured by **S1** and **S2** can be associated with the observation. Both the C1–N vibration in **S1** and the C1=CH_2 vibration in **S2** can be assigned in the regions of around 850 cm^{-1} and around 1650 cm^{-1}, respectively. Moreover, the broadband at 2900 cm^{-1} may cover the newly formed stretching vibration of NH_3^+ in **S2**. Therefore, although the observed Raman spectra did not provide adequate evidences to confirm the coexistence of **S1** and **S2**, the observation does not exclude the possibility that both **S1** and **S2** are formed simultaneously when TNT meets a Cys-capped QD solution.

It should be mentioned that the effect of QDs on the structure and optical absorption of **S1**

and **S2** was not considered in this study. The QDs are usually capped with Cys via bonding with the sulfur atom. Two saturate carbon atoms stand between the sulfur atom and the nitrogen atom that interacts with TNT. Therefore, the sulfur atom and the QD have limited influence on the electronic structures of **S1** and **S2**. Our computations on the TNT-Cys systems are a reasonable approximation for studying the mechanism of TNT detection with amino-capped QDs.

4 Conclusion

In order to reveal the mechanism of TNT detection with amino acid-capped QDs, DFT calculations were performed to study the structures and optical properties of the products of TNT reacting with Cys. A number of candidate structures of TNT-Cys complexes were designed and optimized at the DFT level. Meisenheimer complex (**S1**) and TNT anion (**S2**) were identified as the most stable two structures among the candidates. In previous experimental studies, either **S1** or **S2** had been identified as the product. However, our TDDFT computations for either **S1** or **S2** failed to reproduce the measured spectra. Instead, the superposition of their absorption bands matches well with the measurements. The coexistence of these two complexes was thus suggested and further confirmed in term of their similar thermodynamic stability, and the comparison between predicted and measured Raman spectra. The color change and fluorescence quenching were then interpreted with the optical absorption of both **S1** and **S2**. The absorption bands of **S1** and **S2** are at 451 and 508 nm, respectively, which can be matched by the emission of QDs. Our calculations revealed that the key in the TNT detection is to control the QD size so as to adjust their emission at the wavelength around the absorption bands of the complexes formed with TNT and amino acid.

Acknowledgment

The authors thank financial support from National Natural Science Foundation of China (No. 21373140) and Supported by National High Technology Research and Development Program of China (No. 2015AA034202). Part of calculations was carried out at the State Key Laboratory of Physical Chemistry of Solid Surfaces, Xiamen University.

Notes and references

1 W. D. Won, L. H. Disalvo and J. Ng, *Appl. Environ. Microb.*, 1976, **31**, 576-580.

2 R. Hernandez, M. Zappi and C. H. Kuo, *Environ. Sci. Technol.*, 2004, **38**, 5157-5163.

3 P. van Dillewijn, J. L. Couselo, E. Corredoira, A. Delgado, R. M. Wittich, A. Ballester and J. L. Ramos, *Environ. Sci. Technol.*, 2008, **42**, 7405-7410.

4 O. J. Hao, K. K. Phull, A. P. Davis, J. M. Chen and S. W. Maloney, *Water Environ. Res.*, 1993, **65**, 213-220.

5 S. Singh, *J. Hazard. Mater.*, 2007, **144**, 15-28.

6 M. E. Germain and M. J. Knapp, *Chem. Soc. Rev.*, 2009, **38**, 2543-2555.

7 R. Ban, F. F. Zheng and J. R. Zhang, *Anal. Methods*, 2015, **7**, 1732-1737.

8 W. J. Qi, M. Xu, L. Pang, Z. Y. Liu, W. Zhang, S. Majeed and G. B. Xu, *Chem.-Eur. J.*, 2014, **20**, 4829-4835.

9 B. X. Liu, C. Y. Tong, L. J. Feng, C. Y. Wang, Y. He and C. L. Lu, *Chem.-Eur. J.*, 2014, **20**, 2132-2137.

10 H. X. Zhang, L. J. Feng, B. X. Liu, C. Y. Tong and C. L. Lu, *Dyes. Pigments*, 2014, **101**, 122-129.

11 L. J. Feng, C. Y. Tong, Y. He, B. X. Liu, C. Y. Wang, J. Sha and C. L. Lu, *J. Lumin.*, 2014, **146**, 502-507.

12 S. F. Xu and H. Z. Lu, *Chem. Commun.*, 2015, **51**, 3200-3203.

13 A. Rose, Z. G. Zhu, C. F. Madigan, T. M. Swager and V. Bulovic, *Nature*, 2005, **434**, 876-879.

14 S. J. Toal and W. C. Trogler, *J. Mater. Chem.*, 2006, **16**, 2871-2883.

15 R. Y. Tu, B. H. Liu, Z. Y. Wang, D. M. Gao, F. Wang, Q. L. Fang and Z. P. Zhang, *Anal. Chem.*, 2008, **80**, 3458-3465.

16 W. Wei, X. B. Huang, K. Y. Chen, Y. M. Tao and X. Z. Tang, *RSC Adv.*, 2012, **2**, 3765-3771.

17 L. J. Feng, H. Li, Y. Qu and C. L. Lu, *Chem. Commun.*, 2012, **48**, 4633-4635.

18 R. Freeman, T. Finder, L. Bahshi, R. Gill and I. Willner, *Adv. Mater.*, 2012, **24**, 6416-6421.

19 N. Niamnont, N. Kimpitak, K. Wongravee, P. Rashatasakhon, K. K. Baldridge, J. S. Siegel and M. Sukwattanasinitt, *Chem. Commun.*, 2013, **49**, 780-782.

20 Y. R. Wang, Y. X. Gao, L. Chen, Y. Y. Fu, D. D. Zhu, Q. G. He, H. M. Cao, J. G. Cheng, R. S. Zhang, S. Q. Zheng and S. M. Yan, *RSC Adv.*, 2015, **5**, 4853-4860.

21 L. Liu, J. Y. Hao, Y. T. Shi, J. S. Qiu and C. Hao, *RSC Adv.*, 2015, **5**, 3045-3053.

22 C. L. Zhang, K. J. Wang, D. J. Han and Q. Pang, *Spectrochim. Acta A*, 2014, **122**, 387-391.

23 X. He, H. Wang, Z. B. Li, D. Chen and Q. Zhang, *Phys. Chem. Chem. Phys.*, 2014, **16**, 14706-14712.

24 A. K. M. Jamil, E. L. Izake, A. Sivanesan and P. M. Fredericks, *Talanta*, 2015, **134**, 732-738.

25 H. X. Gu, L. Xue, Y. H. Zhang, Y. F. Zhang and L. Y. Cao, *Adv. Mater. Res.*, 2014, **924**, 366-370.

26 S. S. R. Dasary, A. K. Singh, D. Senapati, H. T. Yu and P. C. Ray, *J. Am. Chem. Soc.*, 2009, **131**, 13806-13812.

27 E. M. A. Ali, H. G. M. Edwards and I. J. Scowen, *Talanta*, 2009, **78**, 1201-1203.
28 D. D. Tuschel, A. V. Mikhonin, B. E. Lemoff and S. A. Asher, *Appl. Spectrosc.*, 2010, **64**, 425-432.
29 H. B. Zhou, Z. P. Zhang, C. L. Jiang, G. J. Guan, K. Zhang, Q. S. Mei, R. Y. Liu and S. H. Wang, *Anal. Chem.*, 2011, **83**, 6913-6917.
30 Z. Z. Guo, A. Florea, C. Cristea, F. Bessueille, F. Vocanson, F. Goutaland, A. D. Zhang, R. Sandulescu, F. Lagarde and N. Jaffrezic-Renault, *Sensor. Actuat. B-Chem.*, 2015, **207**, 960-966.
31 M. C. Casey and D. E. Cliffel, *Anal. Chem.*, 2015, **87**, 334-337.
32 L. L. Zhang, Y. J. Han, J. B. Zhu, Y. L. Zhai and S. J. Dong, *Anal. Chem.*, 2015, **87**, 2033-2036.
33 Y. X. Gan, R. H. Yazawa, J. L. Smith, J. C. Oxley, G. Zhang, J. Canino, J. Ying, G. Kagan and L. H. Zhang, *Mater. Chem. Phys.*, 2014, **143**, 1431-1439.
34 M. Riskin, R. Tel-Vered, T. Bourenko, E. Granot and I. Willner, *J. Am. Chem. Soc.*, 2008, **130**, 9726-9733.
35 X. C. Fu, X. Chen, J. Wang, J. H. Liu and X. J. Huang, *Electrochim. Acta*, 2010, **56**, 102-107.
36 M. Y. Ho, N. D'Souza and P. Migliorato, *Anal. Chem.*, 2012, **84**, 4245-4247.
37 N. Hebestreit, J. Hofmann, U. Rammelt and W. Plieth, *Electrochim. Acta*, 2003, **48**, 1779-1788.
38 C. Carrillo-Carrion, B. M. Simonet and M. Valcarcel, *Anal. Chim. Acta*, 2013, **792**, 93-100.
39 T. Pazhanivel, D. Nataraj, V. P. Devarajan, V. Mageshwari, K. Senthil and D. Soundararajan, *Anal. Methods*, 2013, **5**, 910-916.
40 L. J. Feng, C. Y. Wang, Z. L. Ma and C. L. Lu, *Dyes. Pigments*, 2013, **97**, 84-91.
41 E. Buncel, J. M. Dust and F. Terrier, *Chem. Rev.*, 1995, **95**, 2261-2280.
42 W. S. Zou, D. Sheng, X. Ge, J. Q. Qiao and H. Z. Lian, *Anal. Chem.*, 2011, **83**, 30-37.
43 W. S. Zou, J. Q. Qiao, X. Hu, X. Ge and H. Z. Lian, *Anal. Chim. Acta*, 2011, **708**, 134-140.
44 W. S. Zou, F. H. Zou, Q. Shao, J. Zhang, Y. Q. Wang, F. Z. Xie and Y. Ding, *J. Photochem. Photobiol. A*, 2014, **278**, 82-88.
45 A. Haidour and J. L. Ramos, *Environ. Sci. Technol.*, 1996, **30**, 2365-2370.
46 P. G. Rieger, V. Sinnwell, A. Preuss, W. Francke and H. J. Knackmuss, *J. Bacteriol.*, 1999, **181**, 1189-1195.
47 F. Fant, A. De Sloovere, K. Matthijsen, C. Marle, S. El Fantroussi and W. Verstraete, *Environ. Pollut.*, 2001, **111**, 503-507.
48 Y. F. Chen, Z. Chen, Y. J. He, H. L. Lin, P. T. Sheng, C. B. Liu, S. L. Luo and Q. Y. Cai, *Nanotechnology*, 2010, **21**, 125502.
49 K. Zhang, H. B. Zhou, Q. S. Mei, S. H. Wang, G. J. Guan, R. Y. Liu, J. Zhang and Z. P. Zhang, *J. Am. Chem. Soc.*, 2011, **133**, 8424-8427.
50 W. S. Zou, J. Yang, T. T. Yang, X. Hu and H. Z. Lian, *J. Mater. Chem.*, 2012, **22**, 4720-4727.
51 Y. Q. Wang and W. S. Zou, *Talanta*, 2011, **85**, 469-475.
52 M. J. Frisch, G. W. Trucks, H. B. Schlegel, G. E. Scuseria, M. A. Robb, J. R. Cheeseman, G. Scalmani, V. Barone, B. Mennucci, G. A. Petersson, H. Nakatsuji, M. Caricato, X. Li, H. P.

Hratchian, A. F. Izmaylov, J. Bloino, G. Zheng, J. L. Sonnenberg, M. Hada, M. Ehara, K. Toyota, R. Fukuda, J. Hasegawa, M. Ishida, T. Nakajima, Y. Honda, O. Kitao, H. Nakai, T. Vreven, J. Montgomery, J. A., J. E. Peralta, F. Ogliaro, M. Bearpark, J. J. Heyd, E. Brothers, K. N. Kudin, V. N. Staroverov, R. Kobayashi, J. Normand, K. Raghavachari, A. Rendell, J. C. Burant, S. S. Iyengar, J. Tomasi, M. Cossi, N. Rega, J. M. Millam, M. Klene, J. E. Knox, J. B. Cross, V. Bakken, C. Adamo, J. Jaramillo, R. Gomperts, R. E. Stratmann, O. Yazyev, A. J. Austin, R. Cammi, C. Pomelli, J. W. Ochterski, R. L. Martin, K. Morokuma, V. G. Zakrzewski, G. A. Voth, P. Salvador, J. J. Dannenberg, S. Dapprich, A. D. Daniels, O. Farkas, J. B. Foresman, J. V. Ortiz, J. Cioslowski and D. J. Fox, *Gaussian 09 Revision A.01*, Gaussian, Inc.: Wallingford Ct, 2009.

53 C. Adamo and V. Barone, *J. Chem. Phys.*, 1999, **110**, 6158-6170.

54 Y. Zhao and D. G. Truhlar, *Theor. Chem. Acc.*, 2008, **120**, 215-241.

55 A. D. Becke, *Phys. Rev. A*, 1988, **38**, 3098-3100.

56 C. T. Lee, W. T. Yang and R. G. Parr, *Phys. Rev. B*, 1988, **37**, 785-789.

57 A. D. Becke, *J. Chem. Phys.*, 1993, **98**, 5648-5652.

58 J. D. Chai and M. Head-Gordon, *Phys. Chem. Chem. Phys.*, 2008, **10**, 6615-6620.

59 J. K. Cooper, C. D. Grant and J. Z. Zhang, *J. Phys. Chem. A*, 2013, **117**, 6043-6051.

60 R. Cammi, M. Cossi and J. Tomasi, *J. Chem. Phys.*, 1996, **104**, 4611-4620.

61 R. Cammi, M. Cossi, B. Mennucci and J. Tomasi, *J. Chem. Phys.*, 1996, **105**, 10556-10564.

62 S. F. Xu, H. Z. Lu, J. H. Li, X. L. Song, A. X. Wang, L. X. Chen and S. B. Han, *ACS Appl. Mater. Inter.*, 2013, **5**, 8146-8154.

63 W. S. Zou, Y. Q. Wang, F. Wang, Q. Shao, J. Zhang and J. Liu, *Anal. Bioanal. Chem.*, 2013, **405**, 4905-4912.

Table 1 Calculated bond length (BL, in Å), Wiberg bond order (WBO) and dihedral angle (in degree) of TNT, **S1**, **S2**, **S3** and **S4** in water.

Bond	TNT		**S1**		**S2**		**S3**		**S4**	
	BL	WBO	BL	WBO	BL	WBO	BL	WBO	BL	WBO
C1–C2	1.40	1.36	1.51	0.98	1.48	1.05	1.40	1.36	1.48	1.06
C2–C3	1.38	1.40	1.36	1.52	1.37	1.47	1.39	1.39	1.37	1.54
C3–C4	1.38	1.39	1.40	1.27	1.40	1.31	1.38	1.40	1.40	1.25
C4–C5	1.38	1.39	1.40	1.27	1.41	1.23	1.38	1.37	1.40	1.25
C5–C6	1.38	1.40	1.36	1.52	1.36	1.56	1.38	1.41	1.37	1.54
C6–C1	1.40	1.36	1.52	1.00	1.48	1.05	1.40	1.35	1.48	1.06
C1–C7	1.50	1.03	1.54	0.98	1.34	1.79	1.50	1.04	1.35	1.77
C2–N	1.48	0.90	1.43	1.01	1.42	1.04	1.48	0.90	1.44	0.98
C4–N	1.47	0.91	1.43	1.01	1.43	1.01	1.47	0.91	1.41	1.04
C6–N	1.48	0.90	1.44	1.00	1.44	0.98	1.48	0.89	1.44	0.98
Dihedral angle										
C7–C1–C2–C3		174.6		118.3		150.4		178.3		161.6
O–N–C2–C3		38.3		9.7		11.1		35.1		14.1
O–N–C6–C5		-38.3		-9.4		-26.2		-53.5		-14.0

Table 2 Calculated energy and Gibbs free energy changes (ΔE and ΔG in kcal/mol) of Reactions I and II.

	M06-2X		PBE0	
Reaction	ΔE	ΔG	ΔE	ΔG
I	-3.3	15.8	4.1	22.5
II	2.2	17.7	5.1	20.1

Table 3 Calculated absorption wavelengths (λ, in nm) and oscillator strengths (*f*, in a.u.) of TNT, Cys, **S1**, **S2**, **S3** and **S4**.

	ΔE (S_0-S_1)		ΔE (S_0-S_2)	
	λ	*f*	λ	*f*
TNT	310	0.017	237	0.249
Cys	203	0.041	178	0.016
S1	451	0.219	340	0.388
S2	508	0.155	408	0.366
S3	311	0.010	277	0.014
S4	523	0.157	404	0.348

Figure captions

Scheme 1 Schematic illustration of the two reactions between TNT and Cys.

Fig. 1 TDDFT predicted absorption spectra of TNT calculated at M06-2X(cyan), ωB97XD (green), PBE0 (purple), and B3LYP (red) with the 6-311++G(d,p) basis set.

Fig. 2 Optimized structures of TNT, Cys, **S1**, **S2**, **S3** and **S4** in water solvent.

Fig. 3 Comparison among the experimental (black line) and predicted absorption spectra of **S1** (grey dash line), **S2** (grey solid line) and the combination of **S1** and **S2** at a 1:1 ratio (red line).

Fig. 4 HOMO and LUMO orbitals of TNT, **S1** and **S2**.

Fig. 5 Raman spectra of TNT (a), Cys (b), **S1** (c) and **S2** (d).

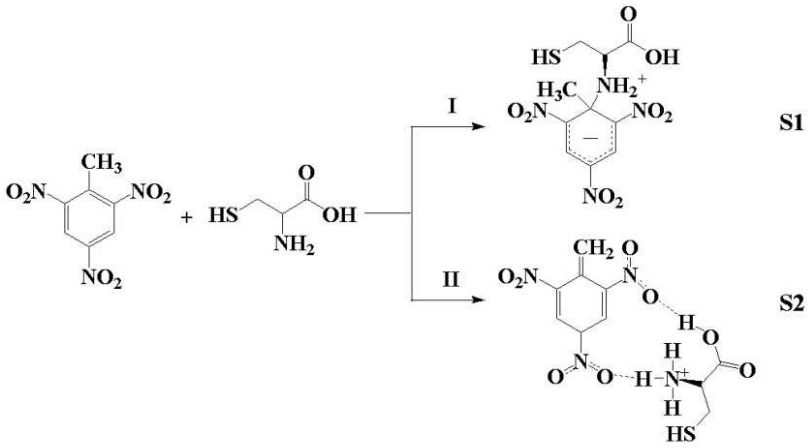

Scheme 1 Schematic illustration of the two reactions between TNT and Cys.

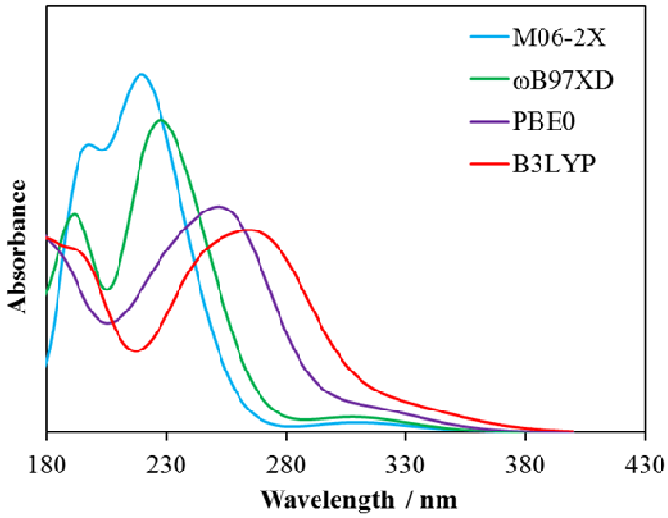

Fig. 1 TDDFT predicted absorption spectra of TNT calculated at M06-2X(cyan), ωB97XD (green), PBE0 (purple), and B3LYP (red) with the 6-311++G(d,p) basis set.

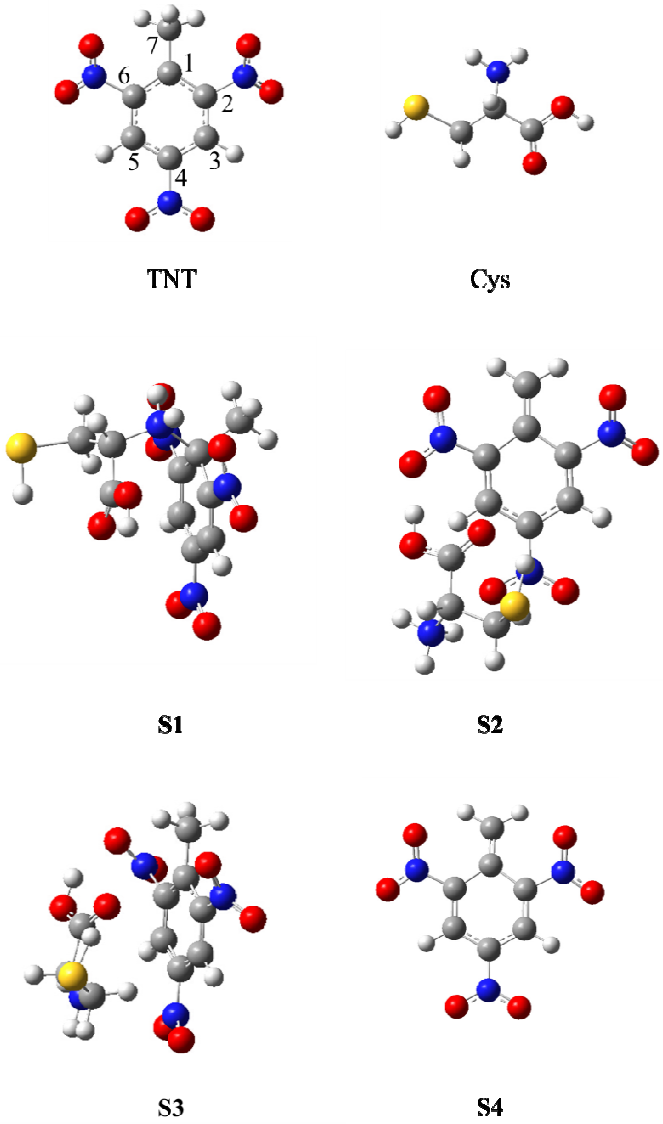

Fig. 2 Optimized structures of TNT, Cys, **S1**, **S2**, **S3** and **S4** in water solvent.

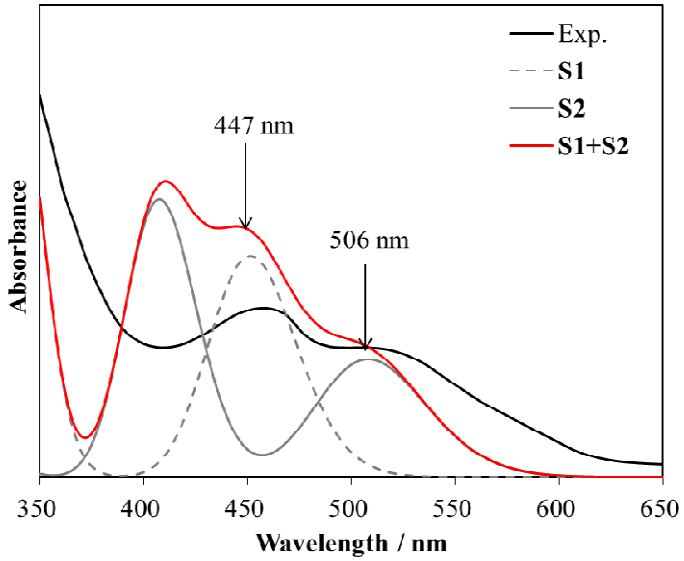

Fig. 3 Comparison among the experimental (black line) and predicted absorption spectra of **S1** (grey dash line), **S2** (grey solid line) and the combination of **S1** and **S2** at a 1:1 ratio (red line).

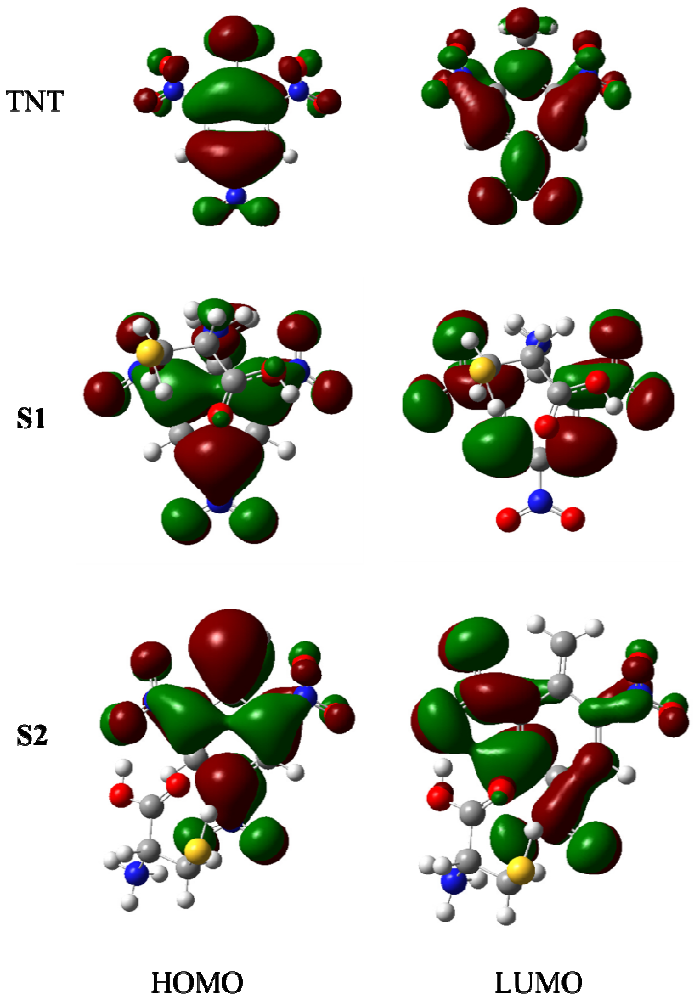

Fig. 4 HOMO and LUMO orbitals of TNT, **S1** and **S2**.

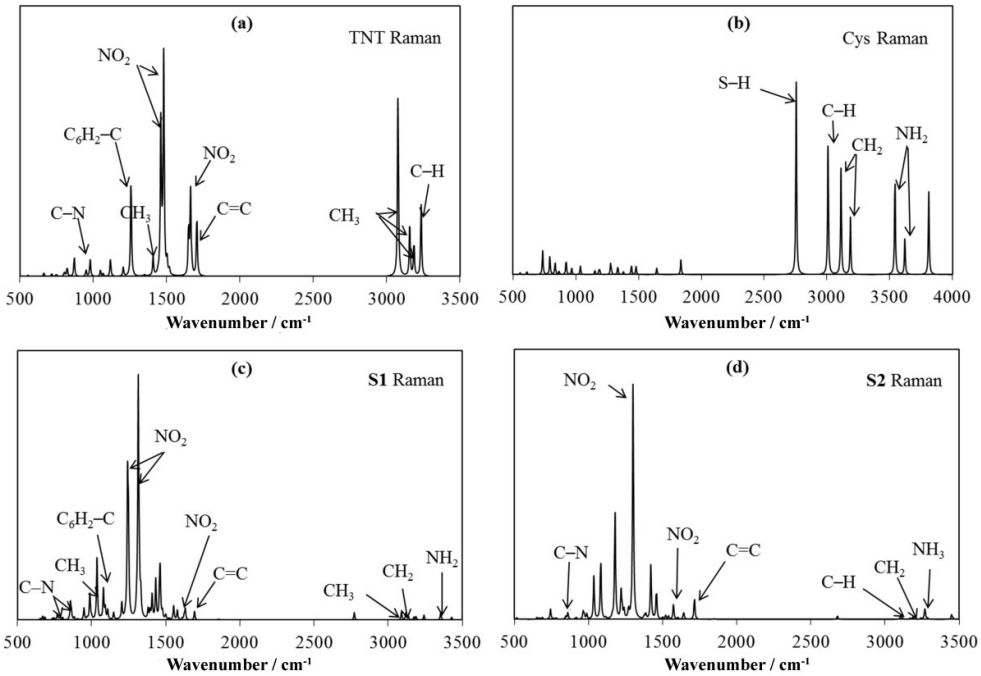

Fig. 5 Raman spectra of TNT (a), Cys (b), **S1** (c) and **S2** (d).

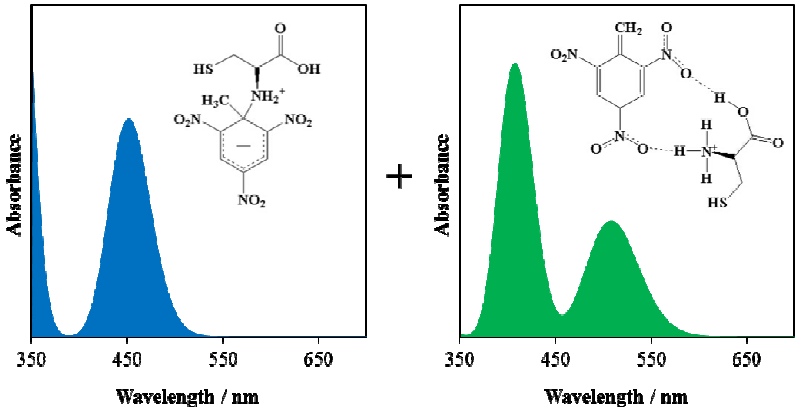

Both Meisenheimer complex and deprotonated TNT are formed when TNT meets amino acid-capped quantum dots.